

LA-UR-82-1433

TITLE: SCANNING ELECTRON MICROSCOPY OF BASALTIC
HYDROMAGMATIC ASH

AUTHOR(S): Kenneth Wohletz and David Krinsley*

SUBMITTED TO: Scanning Electron Microscopy in Geology
Geo Abstracts, Inc.
Norwich England

*Arizona State University, Tempe, AZ 85281

University of California

By acceptance of this article, the publisher recognizes that the U.S. Government retains a nonexclusive, royalty-free license to publish or reproduce the published form of this contribution, or to allow others to do so, for U.S. Government purposes.

The Los Alamos Scientific Laboratory requests that the publisher identify this article as work performed under the auspices of the U.S. Department of Energy.



LOS ALAMOS SCIENTIFIC LABORATORY

Post Office Box 1663 Los Alamos, New Mexico 87545

An Affirmative Action/Equal Opportunity Employer

Scanning Electron Microscopy of Basaltic Hydromagmatic Ash

Kenneth Wohletz
*University of California
Los Alamos National Laboratory
Los Alamos, NM 87545*

David Krinsley
*Department of Geology
Arizona State University
Tempe, AZ 85281*

Abstract

The scanning electron microscope was used to study the surface textures of basaltic hydromagmatic ash from two tuff cones and three tuff rings including Koko Crater, Hawaii; Surtsey, Iceland; Taal Volcano, Philippines; and Kilbourne Hole and Zuni Salt Lake, New Mexico. The textures of 540 ash grains were examined. Ten textural features describe the surface of ash samples: grain morphology, vesicularity, conchoidal fracture, v-shaped depressions, upturned plates, grooves, cracks, adhering particles, chemical alteration, and minor features.

Three stages of ash development are considered: (1) formation by the eruptive process; (2) modification by transport abrasion; (3) alteration by post-emplacement processes. Ash collected from pyroclastic surge deposits shows a higher percentage of broken or planar surfaces than does ash from air-fall deposits which are more vesicular. Surge ash from tuff ring deposits shows a higher percentage of rounding by transport and is generally more altered than associated air-fall ash.

1. Introduction

Scanning electron microscopy (SEM) plays an increasing role in geology as a tool for understanding the nature of particulate matter. During the last 15 years quartz grain surfaces have been studied extensively (Kuenen and Perkok, 1962; Krinsley and Donahue, 1968; Margolis, 1968; and Margolis and Krinsley, 1974). These studies have shown that fine surface textures indicate depositional environment and mode of transport. Heiken (1972, 1974) and

Walker and Croasdale (1972) studied ash using the SEM and related ash morphology to magma composition and eruption type. Honnorez and Kirst (1975) combined SEM along with optical microscopy to develop a system of morphometric quantification. Huang and Watkins (1976) and Huang et al., (1980) have analyzed angular surface pits on deep sea ash particles in order to estimate the frequency of impacts in volcanic eruption columns of silicic composition.

This paper results from a *reconnaissance* investigation of 540 ash particles from 55 samples of basaltic ash collected from tuff cones and tuff rings. The objective of this study is two-fold: 1) to qualitatively delineate major textural features of basaltic ash produced by hydromagmatic (phreatomagmatic) eruptions, and 2) to classify ash textures and relate textural features to the eruptive and emplacement mechanisms of the ash.

Volcanic ash can be produced by one or more of the following mechanisms: (1) explosive vesiculation which ruptures the magma; (1) hydromagmatic eruption where interaction of magma with near-surface water results in fragmentation due to the generation of large thermal or acoustic stresses; and (3) comminution of lava from vent walls during volcanic explosions. Basaltic tuff cones and rings (Heiken, 1971; Wohletz, 1979) result from dominantly hydromagmatic activity; their deposits also contain ash components produced by the other two mechanisms.

In this study, effects of transport and post-emplacement alteration on ash textures are also evaluated. In this way, ash morphology and surface textures fit into a three-stage classification scheme: (1) morphologies indicative of ash formation; (2) textures related to transport abrasion; and (3) types and amounts of alteration.

Honnorez and Kirst (1975) used SEM to distinguish the morphometric parameters of hyaloclastites and hyalotuffs. They found that these ash types, products of submarine hydromagmatic volcanism can be distinguished by grain roundness measured by convexity, concavity, and planarity or by the relationship of the number of grain corners to grain planarity. Ash from hyaloclastites, tuffs occurring with pillow lavas extruded in deep water, has a morphology similar to that of glass artificially granulated by quick chilling. There are more

planar surfaces than on ashes of hyalotuff, which results from near surface steam explosions, an observation similar to that of Walker and Croasdale (1972).

Early SEM studies of volcanic ash show that overall grain morphology is related to the mechanism of ash formation. However, abrasion due to transport may modify the overall grain morphology. The fine abrasion textures on quartz have been studied in detail by Krinsley and Doornkamp (1973). Margolis and Krinsley (1974) and Krinsley and Smalley (1973) have shown that fine textures are generally related to crystal lattice orientation and cleavage planes in quartz. A recent study (Krinsley and others, 1979a) showed that artificially abraded basaltic sand and quartz develop similar fine surface textures. This observation suggests that fine surface features on basaltic glass may be controlled by local glass structures of silicon-oxygen polymers. These small localized areas of order may also produce microlites in the glass. With respect to textures produced by post-emplacement processes, Wise and Weaver (1979) found that ash textures may be identified even after devitrification and diagenesis.

2. Method

Samples were collected from five localities of basaltic volcanism, including Taal Volcano, Philippine Islands, Surtsey, Iceland, Koko Crater, Hawaii, Kilborne Hole, New Mexico and Zuni Salt Lake, New Mexico. Three size fractions were chosen from sieved samples to represent each sample. Sizes used were 354-500 μm , 250-354 μm , and 88-125 μm for those from Taal and Surtsey in order to study size dependency of textures. This size comparison will be presented in a future paper.

Sample washing was performed to remove any organic, loosely adhered, and cementing material. Depending upon the freshness of the grains, washing included soaking in hot, dilute HCl and acetone or cleaning in acetone using ultrasound for not more than 4 minutes so as to preserve grain edges. Samples that were highly palagonitized were destroyed by cleaning in HCl, so only the ultrasound method was used for these samples.

After washing, samples were mounted on stainless steel stubs using doublestick tape. Approximately 10 grains from each of the three size categories were mounted on a single stub. Samples were coated with gold-palladium in order to counteract grain surface charging while scanning with the electron beam. Both whole grain and detailed surface photographs were taken using the secondary electron mode at 25 keV.

3. Geologic Setting

The tuff cones and tuff rings of this study are all basaltic hydromagmatic volcanoes. During eruptions rising magma interacts with near surface water resulting in pulsating steam (Surtseyan) explosions. Fragmented magma is ejected as ash mixed in with expanding steam clouds. Ash is emplaced by pyroclastic surges (base surges) (Moore, 1967; Waters and Fisher, 1971) and air falls. Surges deposits consist of sandwave, massive, and planar bed forms (Sheridan and Up dike, 1975). Wohletz and Sheridan (1979) found that these bed forms are indicators of the density of surge clouds; sandwave, massive and planar beds are deposited in order of increasing surge density. Lower density surges likely result from more explosive eruptions (Wohletz, 1979). However, air falls (Self et al., 1974) are deposited by fallout from an ash-cloud that is ejected initially in a ballistic fashion from the vent. Ash particles in basaltic volcanoes may result from Strombolian eruptions where interaction of surface water is minimal and the magmatic component is dominant.

Tuff rings. Tuff rings are composed of dominantly thin-bedded, poorly indurated surge deposits with small amounts of air-fall tephra. The common sandwave bed forms dominantly occurring near the vent indicate very explosive eruptions. Taal Volcano, Zuni Salt Lake, and Kilbourne Hole are tuff rings that were sampled.

Taal volcano is located in the Philippine Islands and is situated in the middle of Lake Taal, south of Manila. Over 25 recorded eruptions have occurred since 1572 and have been mostly hydromagmatic due to the contact of magma with lake water. The eruptions of 1965 (Moore and others, 1966) produced a tuff ring from which 23 samples of surge tephra were

collected from sandwave, massive and planar beds at distances ranging from 0 to 2 kilometers from the vent.

Zuni Salt Lake (Bradbury, 1967) in west-central New Mexico and Kilbourne Hole (Hoffer, 1976) in southern New Mexico are both maar volcanoes formed in Pleistocene times by basalt magma rising along a fault zone that controlled ground water movement. Both maars are surrounded by tuff rings from which samples of ash deposited as air fall, sandwave, massive and planar surge beds were collected. Eight samples from each location were taken from within 1 kilometer of the crater walls.

Tuff cones. Tuff cones are composed of nearly equal amounts of air-fall ash and planar and massive surge deposits. Near the base of tuff cones, surge deposits predominate and are like ring deposits in that they are poorly consolidated. However, the bulk of a cone is altered to palagonite causing induration. Sandwave bed forms are scarce suggesting that eruptions may have been less explosive due to a greater quenching affect of water (Wohletz, 1979).

Surtsey (Thorarinsson, 1966) is a tuff cone that formed a new island in shallow marine waters south of Iceland in 1964. Koko Crater, Hawaii (Hay and Iijima, 1968) also formed in near-shore marine waters during Pleistocene times. Ash from both cones is palagonitized. Massive and planar surge beds and air-fall beds were sampled, 9 from Surtsey and 8 from Koko crater.

4. Textural Description

Ten textural features were chosen to describe surfaces of the ash samples. These features constitute the most common surface morphologies of basaltic ash determined after reconnaissance observations and considerations of the extensive work done with grain surfaces by Margolis and Krinsley (1974). The essential characteristics identifiable with each microfeature are briefly discussed. Figures were chosen with as much care as possible to illustrate these features.

Grain morphology. The work of Heiken (1972) and Honnorez and Kirst (1975) described the concept of overall grain morphology with respect to basaltic ash. Of the 540 grains studied in this work, three types of morphologies describe most samples: (1) blocky, equant grains with several well-developed planar surfaces resulting from breaking of brittle, quenched lava (Fig. 1); (2) vesicular ash with melted-fused surfaces or fluidal forms of *droplike* textures (Figs. 2 and 3); and (3) vesicular ash with surfaces resulting from rupture of bubble walls (Fig. 4).

Vesicles. All samples contain vesicles (Figs. 4, 5); the degree of vesicularity ranges from nearly zero to nearly 90% by volume. In the studied size range of particles, vesicles range from about 1 μm to 500 μm in diameter, the average being about 100 μm . Vesicles are predominantly the same size within anyone sample. Two populations (generations) of bubbles are rare. Generally, vesicles are spherical but in rare cases form elongated tubes. Those exposed on grain surfaces contain sharp contacts with broken (flat) or conchoidal surfaces, evidence that vesiculation took place before fragmentation.

Unusual features of vesicles are forms that contain a single small pit near the middle of their flat-bottom centers which are associated with solution and precipitation features. Many vesicles have cracked bubble-wall surfaces. These are generally filled with alteration products (Fig. 5).

Conchoidal fractures. These are distinguishing characteristics of glassy materials and quartz, and result from brittle deformation due to compressive contact between two surfaces. In the volcanic environment this situation occurs during transport after magma fragmentation and quenching. Conchoidal fracture patterns (Fig. 6) vary from regular dish shapes (uncommon) to irregular elongate fan-like or trough-like depressions. The common parallel steplike fractures that curve around the conchoidal depression are thought to be expressions of planes of weakness in the glass similar to cleavage planes in crystals (Margolis and Krinsley, 1974). These feather-like fractures that produce a rippled surface texture may also be produced by acoustic wave phenomena (Kragelskii, 1965). Elongate conchoidal fractures are most evident on grain edges.

V-shaped depressions. These are micropits which vary from triangular depressions to elongate grooves that widen in one direction. Chemical effects as well as abrasion quickly obscure these features (Fig. 7). Many of the V-shaped depressions may be only several microns in maximum dimension. These are only evident under magnification of several thousand times.

Two processes can account for the V-shaped depressions: 1) tangential impacts with sliding of one grain over another (Lawn and Wilshaw, 1975), and 2) chemical solution in areas of localized order or microlite development. Huang et al. (1980) consider them to mainly be the result of glancing impacts. They appear to form on all types of tephra particles.

Upturned plates. These features are visible only at magnifications above about 1,000 X (Fig. 8, arrow). Plates resemble subparallel ridges that are slightly raised above the general surface. They form ridgelike structures that are generally less than 10 μm in long dimension. Plate edges are smooth and generally of equal height due to solution/precipitation effects. Plates are found near edges of grains, especially on exposed surfaces as opposed to semi protected hollows. Krinsley and Smalley (1973) have suggested that upturned plates are oriented along traces of cleavage planes in quartz and likely are cleavage plates. Their formation is due to failure along planes of weakness due to mechanical stress applied during impact or crushing.

Grooves. Grooves include elongate scratches and troughs that may be slightly curved. These grooves are oriented in a preferred direction, occur with conchoidal fracture, and appear in sets. Grooves are, however, relatively uncommon on the samples studied.

Transport in a traction carpet is a likely process of formation. Aghan and Samuels (1970) found that, during polishing of metal surfaces, small chips broken from the surface are propelled over surfaces, forming the grooves.

Cracks. Cracks are a very obvious feature of hydromagmatic tephra (Fig. 9), and are straight or slightly curved. Separation along cracks generally is less than 10 μm . Cracks are best developed on vesicle surfaces and may radiate from equal angles in groups of two or four. Overall, these features appear similar to mud cracks (Fig. 10) and, when they intersect, form polygonal plates

on surfaces; they appear to form both before and after conchoidal fracture (Fig. 11). Those that formed previously project through the grain while those that were formed after conchoidal breakage project no more than several microns into grains. Cracks evolve from isolated hairline breaks through stages of intersection with other cracks to pull-aparts of the grain *skin*. Finally plates between cracks curl up at their edges much as do mud cracks and in rare cases reveal a second skin layer beneath. Formation of plates that are only several microns in thickness is of great interest since it suggests that grain surfaces are of slightly different composition than the underlying material (Honnorez and Kirst, 1974). This surface skin may be attributed to a high degree of quenching occurring at grain surfaces, forming a highly glassy "chill zone" or may represent the hydration front of Moore (1966).

Cracks that project through a grain may be due to the thermal stress of quick cooling or by impact with another grain or surface. Cracks in the grain skin could be due to grain expansion after formation of a brittle skin or contraction of the hydrated skin often followed by accumulation of alteration materials (similar to perlitic cracks (Friedman and Smith, 1958).

Adhering particles. Most grains of hydromagmatic origin have surfaces in covered by adhering rounded particles of ash (Fig. 12). The particles range in size from 1 to 20 μm and are either lightly attached or partially fused to the surface of the larger grains. An indistinct trend toward fewer adhering particles occurs in samples collected from beds of coarser median grain size. These particles of ash represent the micron and smaller size-fraction of ash produced during eruption and are scavenged from the eruption cloud by the larger particles. It is difficult to estimate their volume but it is important to note their existence and compare them to Heiken's (1972) magmatic samples which do not appear to have adhering particles. During volcanic transport, small particles may agglutinate to larger ones due to cohesiveness of wet surfaces or electrostatic charging due to breakage (Krinsley and Leach, 1979b).

Chemical alteration. Palagonitization is a process of basaltic glass hydration (Moore, 1966). By-products of this process are zeolites, calcite, and clays (Hay and Iijima, 1968). Under the optical microscope, palagonite is vitreous, wax-like, or resinous and varies in color from white to orange to orange to tan. Palagonitization is most apparent in vesicles (Fig. 13) where accumulations of

small zeolite or clay crystals occur. Palagonitization shows progressive degrees of development from production of a hydrated skin on vesicle surfaces (Fig. 14) to partial in-filling of vesicles by small crystals. Palagonitized grain surfaces take on a white tinge under SEM. Grains are sugary in appearance when totally altered; however, they retain their vesicular morphology.

Micrographs of completely palagonitized grains demonstrate that palagonite does not destroy original grain boundaries.

Solution and precipitation occur together on the same grain (Fig. 14). Resulting textures include pitted or scalloped surfaces on a micron scale, rounding of upturned plates or other sharp features, and development of a frosted, light diffused surface as compared to the vitreous surface of fresh glass.

Minor features. Alignment of very small (~1 to 10 μm) vesicles along linear (~10 to 100 μm) scarps that cross grain surfaces are rare. Scarps are small linear displacements which appear on flat grain surfaces (Fig. 15). Tiny bubbles exist along scarp bases; all the bubbles are the same size and are smaller by one or two orders of magnitude than the average bubble size normally found in grains. These small bubbles appear to be evidence of a late-state vesiculation event related to scarp formation.

Another feature that is more common is foliation of banded grains. This feature is attributed to viscous shear deformation of the lava near its solidus temperature prior to fragmentation (Fig. 16).

5. Textural Analysis

Table 1 summarizes important textural features with respect to developmental stage. Three stages are considered in order to classify grains by texture: formation, transport, and alteration. Table 2 is a classification of all samples by individual grain counts. This data is presented in Figs. 17-21, and is plotted as percentages of textural-type versus bed form. The bed forms shown left to right on the plots are sandwave, massive, planar, and air fall in order of increasing median diameter of ash in each deposit-type determined by previous studies (Wohletz,

1979; Sheridan and Wohletz, in press). the transition from planar to air fall marks a change from vapor-supported surge deposition of ash to non-supported ballistic transport of coarse ash and lapilli.

TABLE 1. Classification of Basaltic Ash Morphology and Textures

Ash formation mechanism	Transport	Alteration
▶ Surface planarity	▶ overall grain rounding	▶ palagonitization
▶ vesicularity	▶ conchoidal fracture	▶ solution and precipitation
▶ fused skin or drop-like texture	▶ v-shaped depressions	▶ skin cracks
▶ deformation planes	▶ upturned plates	
▶ adhering particles	▶ grooves	
	▶ cracks	

Ash formation. Ash morphology is characterized by the nature of its bounding surfaces. Three morphology types characterize most ash: fused or drop-like surfaces (D); planar and broken surfaces (8); and surfaces formed by bubble walls of vesicular ash (V). Each grain is considered to have a dominant morphology characterized by one of the above. Figure 17 shows the distinct trend toward an increase in vesicularity and decrease of surface breakage and fusion for ash transported ballistically and deposited by fallout from an ash cloud. However, where ring and cone samples are considered separately (Fig. 18) this trend is complicated because cones show an opposite trend to that followed by ring ash: breakage increases and vesicularity decreases slightly.

Transport. Five fine surface features given in Table 1 are related to transport; these features result from grain to grain-to-substrate collisions. Due to the reconnaissance nature of this work, individual grains were not classified as to the presence or absence of these features. However, abrasion due to transport is easily classified by noting the presence (R) or absence (A) of

roundness (Table 2). Figure 19 is a plot of ash rounding with trends shown for ring and cone samples, and as in Fig. 18, rings show an opposite trend to cones.

Alteration. The alteration stage coincides with: 1) formation of microcrystalline palagonite which adheres to vesicle surfaces; 2) solution and precipitation; 3) hydration of glassy rinds; and 4) subsequent cracking of hydrated materials. Alteration is classified by degree: (0) non-altered where no microcrystalline material or hydration is evident; (1) partly altered where vesicles are filled with alteration; and (2) totally altered where the entire surface of the grain is covered by alteration, cracks occur in the hydrated skin, and the grain takes on a sugary appearance. The interpretation of alteration degree may be very dependent upon the deposit age. However, Jakobsson (1972) found that palagonitization occurs shortly after eruptions cease. This consideration allows for a comparison of alteration among the studied localities. Figure 20 shows that alteration decreases for planar and air-fall beds and is overall highest in massive surge beds. Figure 21 separates the alteration of cones and rings. Again, cones show an -opposite trend from rings for the amount of alteration when moving from the surge to air-fall fields.

Ash Classification. A simple means of classifying ash samples based upon the above criteria is facilitated by Table 3, and consists of a tripartite classification. The first character (Morphology %) refers to the dominant morphology; the 80% level is considered as the minimum value for dominance of broken morphology. The second character represents alteration (0,1,2) where 1-60% is chosen as the minimum degree of dominance for non-altered ash, and 15% as the minimum for dominance of 2 (partly altered ash). A figure of 20% is the minimum for the sample to be characterized as rounded. Using this scheme, the following generalized classification of tephra results.

Bedform	Cones	Rings
Sandwave Beds	▶ Absent	▶ Broken, partly altered, angular (B1A)
Massive Beds	▶ Broken, totally altered, rounded (B2R)	▶ Broken, partly altered, rounded (B1R)
Planar Beds	▶ Vesicular, partly altered, angular (V1A)	▶ Broken, nonaltered, rounded (B0R)
Air-fall Beds	▶ Vesicular, nonaltered, angular (V0A)	▶ Vesicular, partly altered, angular (V1A)

6. Discussion

Due to the reconnaissance nature of this study textural analysis gives only preliminary results. However, the data are consistent in showing a difference in texture between surge and air-fall transported ashes.

Air-fall ashes are coarser-grained and better sorted than are surge tephra. Field studies show that air-fall ashes from basaltic tuff rings and tuff cones are dominantly magmatic in origin (Wohletz, 1979; Wohletz and Sheridan, in press). SEM analysis supports this hypothesis that vesicularity increases and breakage characteristic of water interaction decreases for air fall ashes. Self and Sparks (1979) have shown that in phreatoplinian eruptions producing hydromagmatic surge and air-fall products, the air-fall ash is much finer-grained than in purely magmatic Plinian eruptions. The hydromagmatic mechanism tends to be much more effective in production of fine ash. The presence and abundance of ultra-fine ash adhering to grain surfaces of samples may give clues to size distributions in hydromagmatic eruption columns where ash cohesion is large.

Rounding or transport abrasion is largely dependent upon the distance of transport. Wohletz and Sheridan (1979) found that tephra existing in planar beds is generally transported the greatest distance from tuff ring vents. Tephra from massive and sandwave beds travel

successively shorter distances. The degree of rounding shown in Fig. 19 indicates that planar-bed ash does show the most abrasion. However, in tuff cones where surges must travel up steep slopes to escape from the crater, planar bed tephra shows less rounding. This trend may indicate that poorly inflated surges depositing planar beds travel only a short distance from the vents in tuff cones. Abrasion of air-fall lapilli is likely the result of post emplacement avalanching of materials.

Palagonitization of ash is thought to occur in tuff rings and cones due to groundwater moving through the deposits (Hay and Iijima, 1968) or post-eruptive hydrothermal fluids emanating from the vent (Jacobsson, 1972). However, SEM results show that air fall ashes are least altered and massive surge sheets are most greatly altered. These two deposit-types are interbedded in cones. Therefore consideration of emplacement mechanisms suggests the following explanation of alteration. Since air-fall ashes differ from surge ashes in that they are not emplaced in a steam-rich cloud, it is likely that they are drier upon emplacement. Planar beds are deposited from surges that are poorly inflated by steam relative to those depositing massive beds and show less alteration than massive surge ashes. It follows that the wetness upon emplacement of hydromagmatic deposits controls the degree of post emplacement alteration while the ash is still warm.

The opposite textural trends noted for cones and rings are difficult to evaluate and data presented here is insufficient to satisfactorily explain trends. However, these opposing textural trends do support a hypothesis that these volcanoes follow differing evolutionary patterns (Wohletz, 1979; Wohletz and Sheridan, 1980).

7. Conclusions

Scanning electron microscopy provides a method of classifying volcanic ash based upon surface morphology and texture. For samples of basaltic ash collected from tuff cones and tuff rings the following textures describe ash surfaces. Surface planarity, vesicularity and fused skin or drop-like texture are a result of an eruptive mechanism. Overall grain rounding consisting of

conchoidal fracture, v-shaped patterns, upturned plates, grooves and cracks projecting through the grain results from the transport and emplacement process. Finally, palagonitization, hydration, skin cracks, and solution and precipitation are textures of post-emplacement alteration.

The degree of surface planarity or breakage is greater for ashes emplaced during hydromagmatic eruptions where transport occurs via base surge. Ash vesicularity increases for air-fall ashes which may result from magmatic phases of activity.

The degree of grain rounding and alteration depends upon bed form and vent type and is generally greater for ash of surge deposits than air-fall deposits. However, this relationship is highly dependent upon whether the sample is from a tuff cone or tuff ring.

Although this study constitutes only a reconnaissance of basaltic ash textures it does indicate that the SEM can be a useful tool in determining the nature of explosive volcanic eruptions and perhaps can be used for eruption prediction.

8. Acknowledgements

This research was supported by NASA Consortium Agreement 2-0R035-801 and 2-0R035-901, NASA grants NSG-7642 and NAGW-24, Office of Planetary Geology. We wish to thank Stephen Self, Johan Varekamp, Grant Heiken, and Michael Sheridan for reviewing the manuscript. Michael Sheridan supplied samples of Taal and Surtsey ash together with descriptions of sample locations and geology. Special thanks go to Ellen Patera who printed and labeled over 500 photographs taken in this study and Sue Selkirk for drafting the figures.

9. References

- Aghan, R. L. & Samuels, L. E., 1970, Mechanisms of abrasive polishing: *Wear*, v. 16, p. 293-301.
- Bradbury, J. P., 1967, origin, paleolimnology, and limnology of Zuni Salt Lake maar, west central New Mexico: Ph.D. Dissertation, University of New Mexico, 246 p.
- Friedman, I. I., & Smith, R. L., 1958, The deuterium content of water in soluble volcanic glasses: *Geochimica et Cosmochimica Acta*, v. 15, p. 218-228.

- Hay, R. L. & Iijima, A., 1968, Nature of origin of palagonite tuffs of the Honolulu Group on Oahu, Hawaii: Geological Society of America Memoir 116, p. 331-376.
- Heiken, G., 1971, Tuff rings: examples from the Fort Rock -Christmas Lake Valley basin, south central Oregon: Journal of Geophysical Research, v. 76, p. 5615-5626.
- Heiken, G., 1972, Morphology and petrography of volcanic ashes: Geological Society of America Bulletin, v. 83, p. 1961-1988.
- Heiken, G., 1974, An atlas of volcanic ash: Smithsonian Contributions to Earth Science, v. 12, p. 1-101.
- Hoffer, J. M., 1976, The Potrillo basalt field, south central New Mexico: New Mexico Geological Society Special Publications, v. 5, p. 89-92.
- Honnorez, J., & Kirst, P., 1976, Submarine basaltic volcanism: Morphometric parameters for discriminating hyaloclastites from hyalotuffs: Bulletin of Volcanology, v. 34, p. 1-25.
- Huang, T. C. & Watkins, N. D., 1976, Volcanic dust in deep-sea sediments: relationship of microfeatures to explosivity estimates: Science, v. 193, p. 576-579.
- Huang, T. C., Varner, J. R. & Wilson, L., 1980, Micropits of volcanic glass shards: laboratory simulation and possible origin: Journal of Volcanology and Geothermal Research, v. 8, p. 59-68.
- Jakobsson, S. P., 1972, on the consolidation and palagonitization of the tephra of the Surtsey Volcanic Island, Iceland: Surtsey Progress Report, v. IV, p. 121-128.
- Kragelskii, I. V., 1965, Friction and Wear: Butterworths, London, 225 p.
- Krinsley, D. H. & Donahue, J., 1968, Environmental interpretation of sand grain surface textures by electron microscopy: Geological Society of America Bulletin, v. 79, p. 743-748.
- Krinsley, D. H. & Doornkamp, J., 1973, Atlas of Quartz Sand Grain Textures: Cambridge University Press, Cambridge, England, 91 p.
- Krinsley, D. H., Greeley, R., & Pollack, J. B., 1979a, Abrasion of windblown particles on Mars -erosion of quartz and basalt sand under simulated martian conditions: Icarus, v. 39, p. 364-384.
- Krinsley, D. H., & Leach, R., 1979b, Simulated martian aeolian abrasion and the creation of "aggregates": Reports of the Planetary Geology Program, 1978-1979, NASA Technical Memo 80339, p. 313-315.
- Krinsley, D. H. & Smalley, I. J., 1973, Shape and nature of small sedimentary quartz particles: Science, v. 180, p. 1277-1279.
- Krinsley, D., & Wellendorf, W., 1980, Wind velocities determined from the surface textures of sand grains: Nature, v. 283, p. 372-373.
- Kuenen, Ph. H., and Perdok, W. G., 1962, Frosting and defrosting of quartz sand grains: Journal of Geology, v. 70, p. 648-658.
- Lawn, B. R. & Wilshaw, T. R., 1975, Review indentation fracture: principles and applications: Journal of Material Science, v. 10, p. 1049-1081.
- Margolis, S. v., 1968, Electron microscopy of chemical solution and mechanical abrasion features on quartz sand grains: Sedimentary Geology, v. 2, p. 243-256.
- Margolis, S. V. & Krinsley, D. H., 1974, Processes of formation and environmental occurrence of microfeatures of detrital quartz grains: American Journal of Science, v. 274, p. 449-464.
- Moore, J. G., 1974, Rate of palagonitization of submarine basalt adjacent to Hawaii, in Geological Research 1966 - United States Geological Survey Professional Paper 550-0, p. 163-171.
- Moore, J. G., 1967, Base surge in recent volcanic eruptions: Bulletin Volcanologique, v. 30, p. 337 -363.
- Moore, J. G., Nakamura, K., & Alcaraz, A., 1966, The 1965 eruption of Taal Volcano: Science, v. 151, p. 955-960.

- Self, S., Sparks, R. S. J., Booth, B., and Walker, G. P. L., 1974, The 1973 Heimaey strombolian scoria deposit, Iceland: *Geological Magazine*, v. III, p. 539-548.
- Self, S. & Sparks, R. S. J., 1978, Characteristics of widespread pyroclastic deposits formed by the interaction of silicic magma and water: *Bulletin Volcanologique*, v. 41, p. 1-17.
- Sheridan, M. F. & Wohletz, K. H., in press, Particle size characteristics of surge deposits: *Bulletin Volcanologique*.
- Sheridan, M. F., & Up dike, R. G., 1975, Sugarloaf Mountain tephra a Pleistocene rhyolitic deposit of base surge origin: *Geological Society of America Bulletin*, v. 86, p. 571-581.
- Thorarinsson, S., 1966, Surtsey the new island in the North Atlantic: *Almenna Bokafelagid, Reykjavik*, 47 p.
- Walker, G. P. L., 1973, Explosive volcanic eruptions -a new classification scheme: *Geologisches Rundschau*, v. 62, p. 431-446.
- Walker, G. P. L., & Croasdale, R., 1972, Characteristics of some basaltic pyroclastics: *Bulletin Volcanologique*, v. 35, p. 305-317.
- Waters, A. E. & Fisher, R. V., 1971, Base surges and their deposits: Capelinhos and Taal Volcanoes: *Capelinhos and Taal Volcanoes: Journal of Geophysical Research*, v. 76, p. 5596-5614.
- Wise, S. W. & Weaver, F.M., 1979, Volcanic ash: examples of devitrification and early diagenesis: *Scanning Electron Microscopy*, v. 1, p. 511-518.
- Wohletz, K. H. & Sheridan, M. F., 1979, A model of pyroclastic surge: *Geological Society of America Special Paper 180*, p. 177-193.
- Wohletz, K. H., 1979, Evolution of tuff cones and tuff rings: *Geological Society of America Abstracts with Programs*, v. 11, p. 543.

TABLE 1.
(In the text above)TABLE 2.
Textural Description of Samples

Sample/Bedform	Morphology			Alteration			Roundness	
	D	B	V	0	1	2	R	A
<u>Taal</u>								
T-19 S	1	8	0	8	1	0	1	8
T-21 S	0	10	0	5	5	0	3	7
T-13 S	0	8	0	2	1	0	2	6
T-11 S	0	7	2	3	6	0	1	8
T-23 S	0	7	0	4	3	0	3	4
T-6 S	1	9	0	9	0	1	3	7
T 5 S	0	8	0	4	3	1	1	7
T-3 S	0	9	0	6	3	0	0	9
T-2 S	0	10	0	6	4	0	0	10
T-24 M	4	1	4	8	1	0	0	9
T-20 M	1	9	0	10	0	0	0	10
T-18 M	1	7	1	8	1	0	2	7
T-17 M	2	8	0	7	3	0	3	7
T-15 M	2	9	0	22	0	0	1	10
T-14 M	0	7	0	6	1	0	2	5
T-8 M	0	8	0	5	3	0	1	7
T-4 M	0	10	0	9	1	0	3	7
T-1 M	0	9		7	3	0	1	9
T-15 P	3	11	2	12	2	2	4	12
T-12 P	0	9	0	4	4	1	2	7
T-10 P	0	10	0	9	1	0	1	9
T-7 P	0	9	1	9	1	0	2	8
<u>Kilbourne Hole</u>								
KH-8B S	1	8	0	0	5	2	0	7
KH-1A S	0	7	0	2	5	0	0	7
KH-8C S	1	4	0	0	3	2	0	5
KH04B S	0	7	0	2	5	0	0	8
KH-8A M	1	8	2	0	7	4	5	6
KH-7 M	0	9	2	0	6	5	3	8
KH-4A AF	0	5	1	0	1	2	1	7
KH-1B AF	0	6	2	4	4	0	1	7
<u>Zuni Salt Lake</u>								
Z-2B S	0	7	2	6	3	0	1	8
Z-2A S	0	6	12	14	4	0	0	18
Z-1B S	1	5	1	1	6	0	2	5
Z-1A M	0	11	1	1	5	5	6	5
Z-3B M	0	9	0	0	9	0	2	7
Z-5A P	0	4	0	3	3	3	0	9
Z-2A P	1	8	1	7	3	0	5	6

TABLE 2 (Cont.).

Sample/Bedform	Morphology			Alteration			Roundness	
	D	B	V	0	1	2	R	A
Surtsey								
S-10 M	1	9	0	a	4	2	4	4
S9 M	1	7	0	6	2	0	3	5
S6 M	1	9	0	3	3	4	6	4
S5 M	3	6	1	5	4	2	0	1
S3 M	0	8	0	4	4	0	3	8
S1 M	0	8	2	8	2	0	5	5
S-11 P	3	2	5	2	6	2	0	1
S2 P	1	8	1	7	3	0	3	7
Koko Crater								
KC-1B M	0	3	0	0	6	3	3	0
KC-11 M	1	10	0	1	8	2	8	3
KC-10 M	0	4	0	1	3	0	2	2
KC-6A M	0	8	3	5	6	0	2	9
KC-1A P	0	8	1	3	6	0	2	7
KC-3A AF	1	7	0	4	4	0	4	4
KC-6B AF	0	4	4	5	3	0	1	7
KC-6C AF	0	7	2	6	1	2	2	7

Morphology: D = drop-like, B = broken, V = vesicular

Alteration: 0 = none, 1 = partial, 2 = total

Roundness: R = rounded, A = angular

In the first column, Sample Bedform, the letter(s) following the sample number are represented as follows:

S = Sandwave Beds

M = Massive Beds

P = Planar Beds

AF = Airfall Beds

TABLE 3. Classification of Ash
Samples by Vent and Deposit Type

Vent Bedform	Morphology%			Alteration%			Roundness %
	D	B	V	0	1	2	R A
<u>Cones</u>							
10 M	9	84	7	41	44	15	40 60
4 P	10	62	28	41	54	5	12 88
3 AF	4	72	24	60	32	8	28 72
Total	8	77	17	44	45	9	31 69
<u>Rings</u>							
16 S	5	83	12	53	42	5	12 88
13 M	9	83	8	57	31	12	23 77
7 P	6	87	7	65	26	9	23 77
2 AF	0	78	22	50	50	0	14 86
Total	6	83	11	57	35	8	17 83

Morphology: D = drop-like, B = broken, V = vesicular

Alteration: 0 = none, 1 = partial, 2 = total

Roundness: R = rounded, A = angular

In the first column, Vent Bedform, the letter(s) following the numbers are represented as follows:

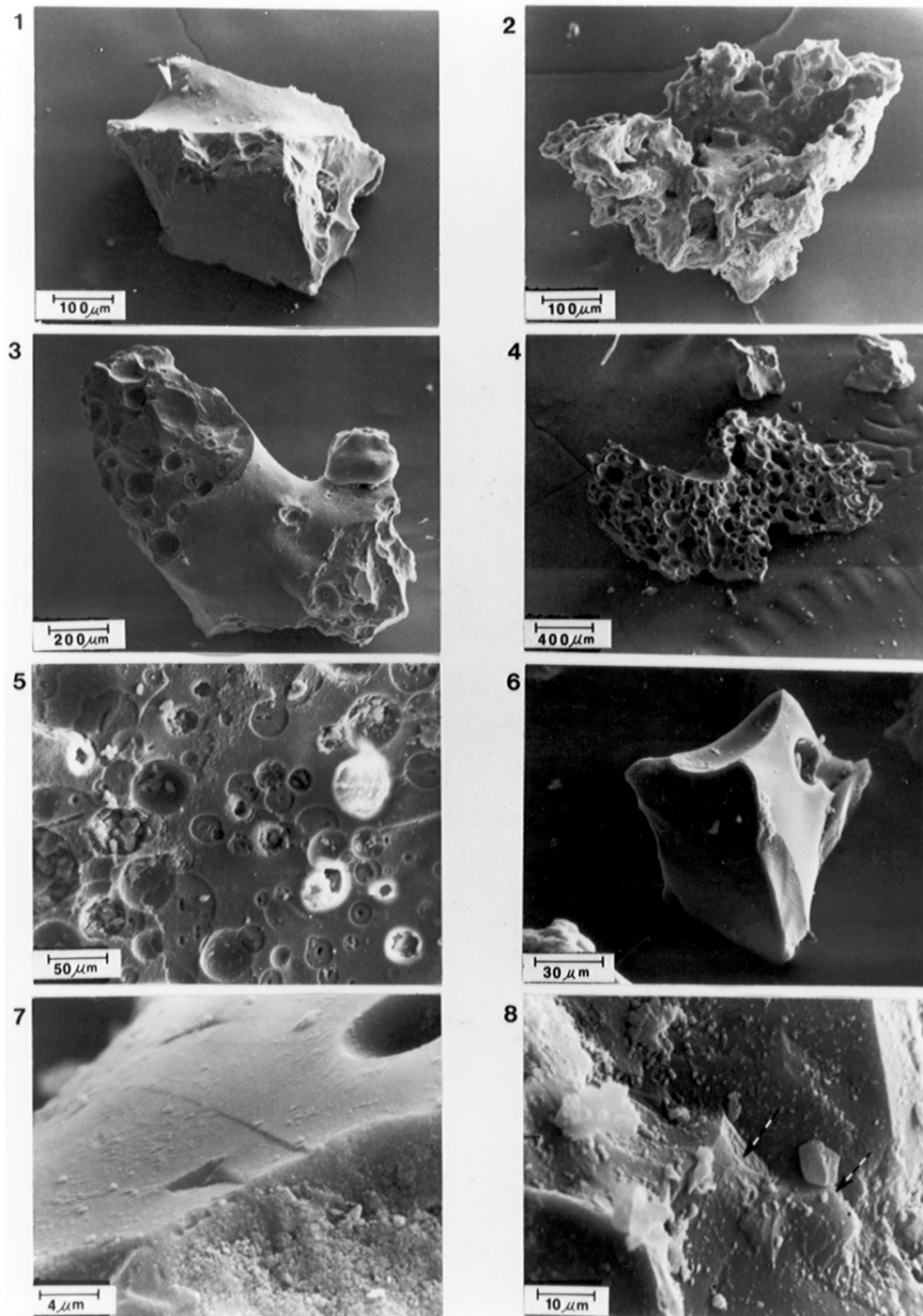
S = Sandwave Beds

M = Massive Beds

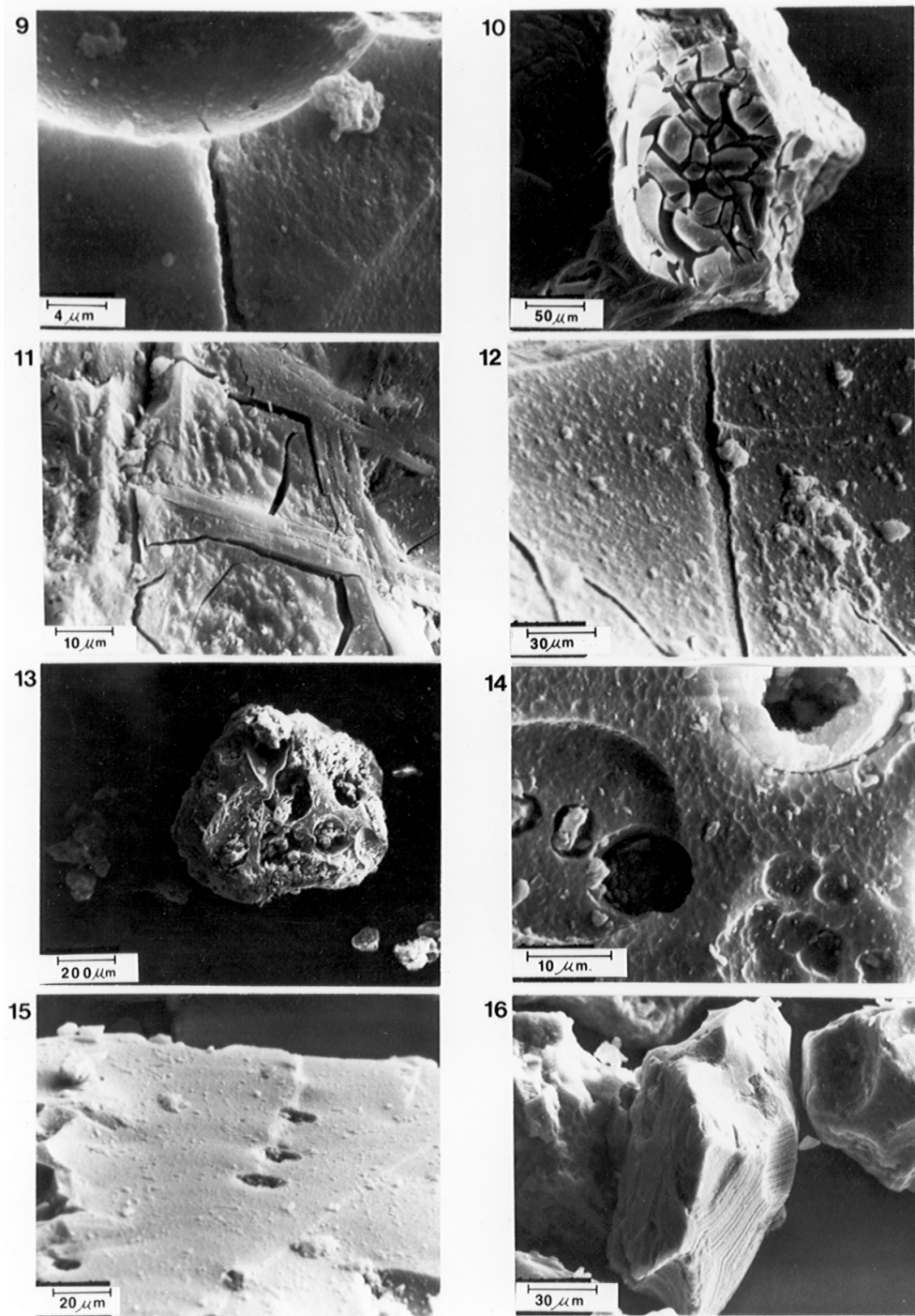
P = Planar Beds

AF = Airfall Beds

The numbers in front of the letters represent the number of samples examined.



Figures 1-8: 1) T-5, Blocky, equant morphology showing broken surfaces. Sample location and deposit type given by sample number in Table 2. 2) 5-11, Vesicular ash with fused surface. 3) T-17, Drop-like or fluidal form ash. 4), Highly vesicular ash with surface resulting from bubble-wall texture. 5) T-II, Flat-bottomed vesicles with small indentations at their centers associated with vesicles filled with palagonite. 6) KC-6C, Elongate conchoidal fractures with subsidiary step-like cleavage on grain corner. 7) T-8, V-shaped depression developed on flat surfaces. 8) T-II, Upturned plates visible along fracture surface in lower right portion of the picture (arrow).



Figures 9-16: 9) KC-6C, Crack extending radially from vesicle center and projecting into the grain. 10) S-6, Mudcrack-like texture of altered (hydrated) glass skin lining vesicle surface. 11) S-10, Two generations of cracks related to altered skin, and possible feldspar microlite orientation. 12) S-9, Adhering particles forming mound-like irregularities on grain surface. Crack formed by "pull-apart" of hydrated skin appears to have occurred after attachment of small particles. 13) KC-1B, Palagonite alteration manifested by numerous crystallites which fill in vesicles and form crusty patches between them. 14) T-II, Solution and precipitation pits formed on the surface of the grain pictured in Fig. 5. Also note vesicles. Scalloping due to solution tends to destroy vesicle outline. 15) T-8, Alignment of small incipient vesicles along a curved deformation plane. 16) KC-6C Foliation due to viscous flow of lava prior to fragmentation.

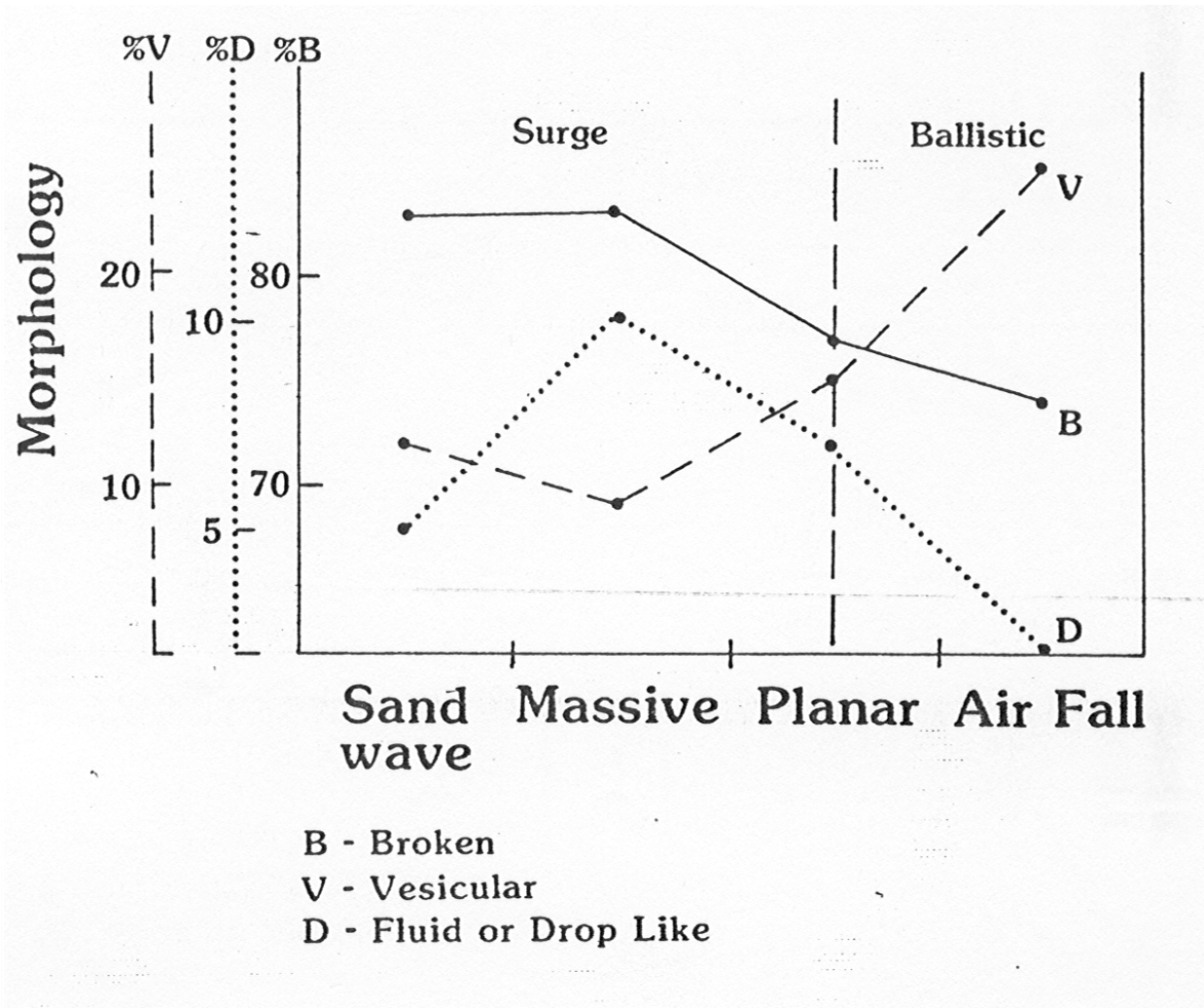


Figure 17: Plot of percentage of broken (B), vesicular (V), and fluidal or drop-like (D) ash versus bed form, sandwave (S), massive (M) and planar (P) surge, and air fall (AF).

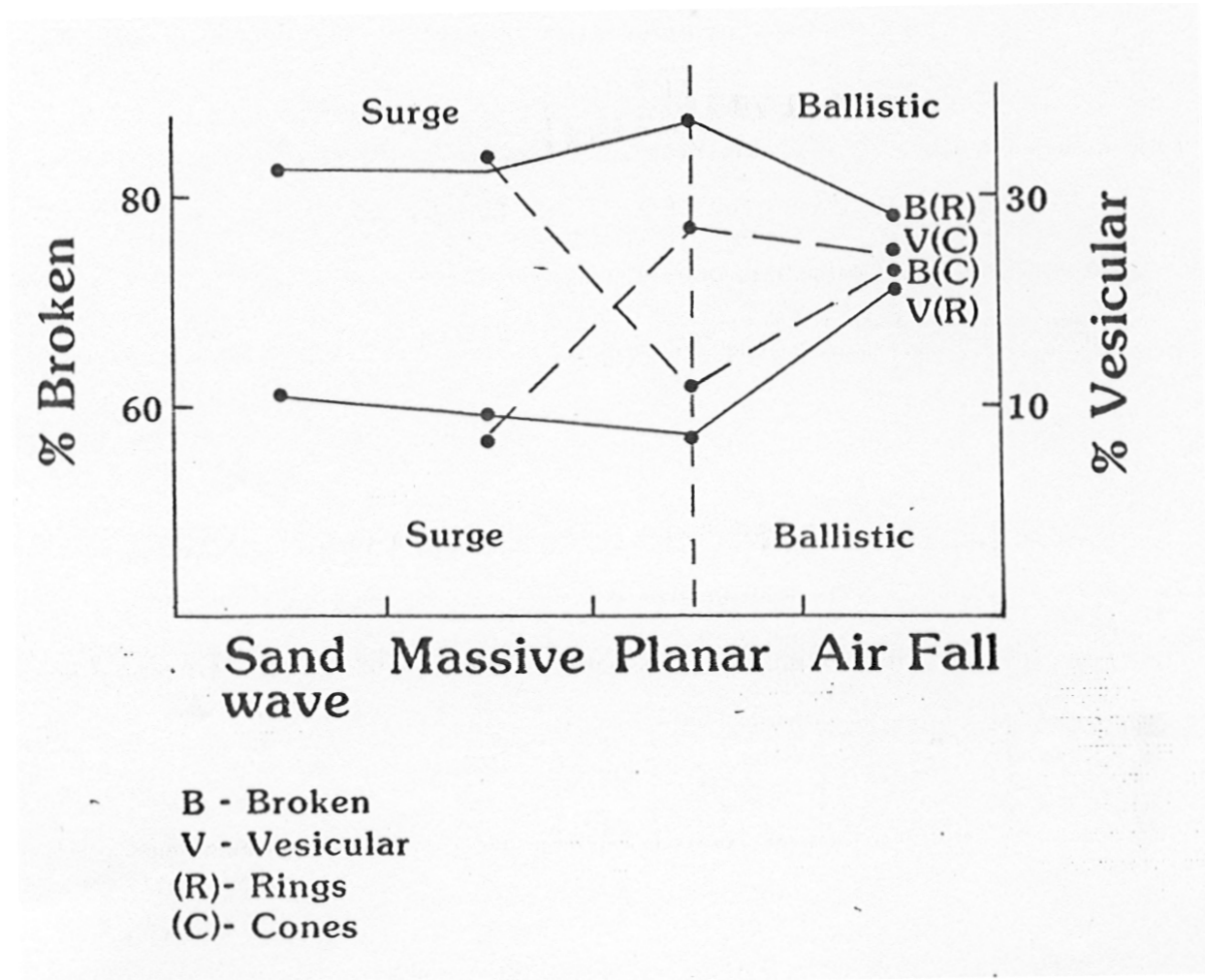


Figure 18: Plot of B and V percentage versus bedform for tuff cones (C) and tuff rings (R).

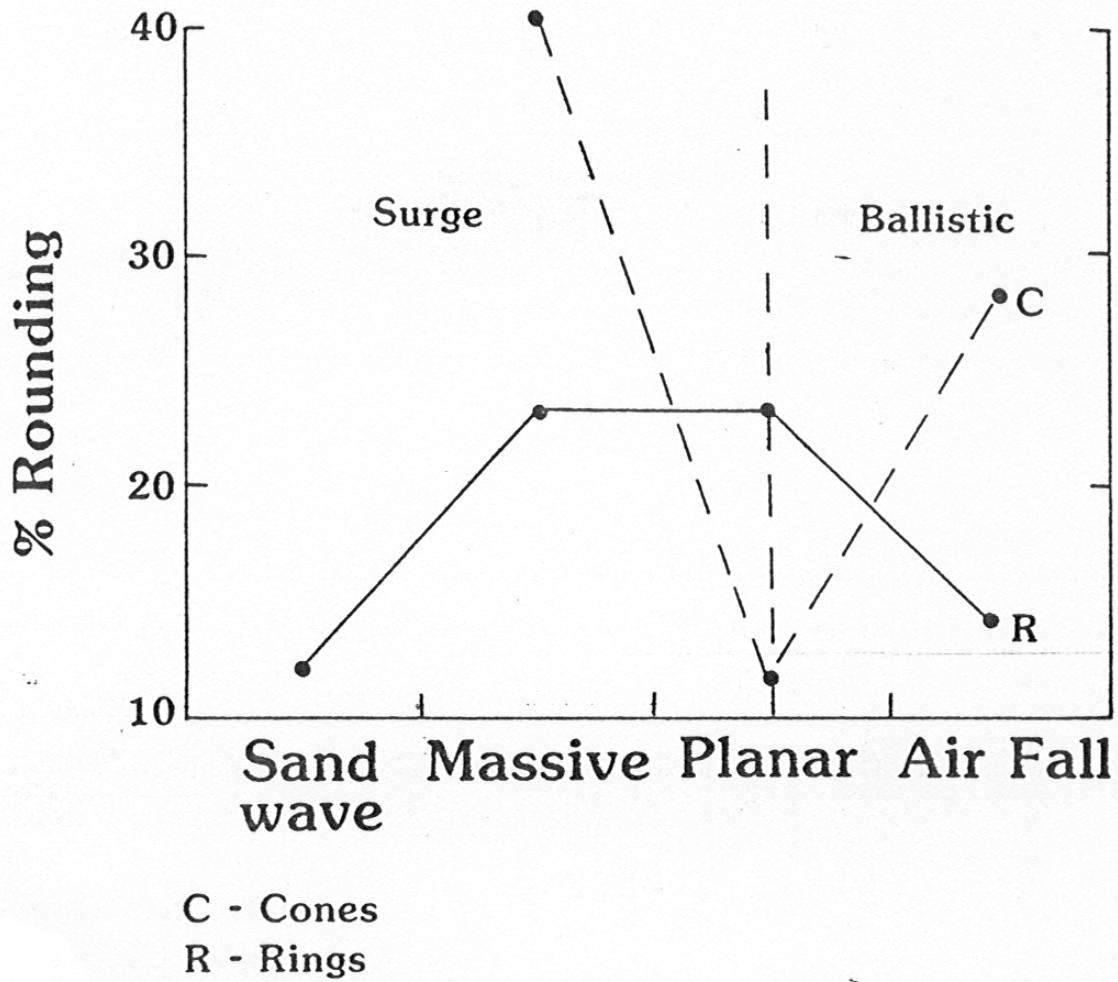


Figure 19: Plot of rounded ash percentage versus bedform for cones and rings.

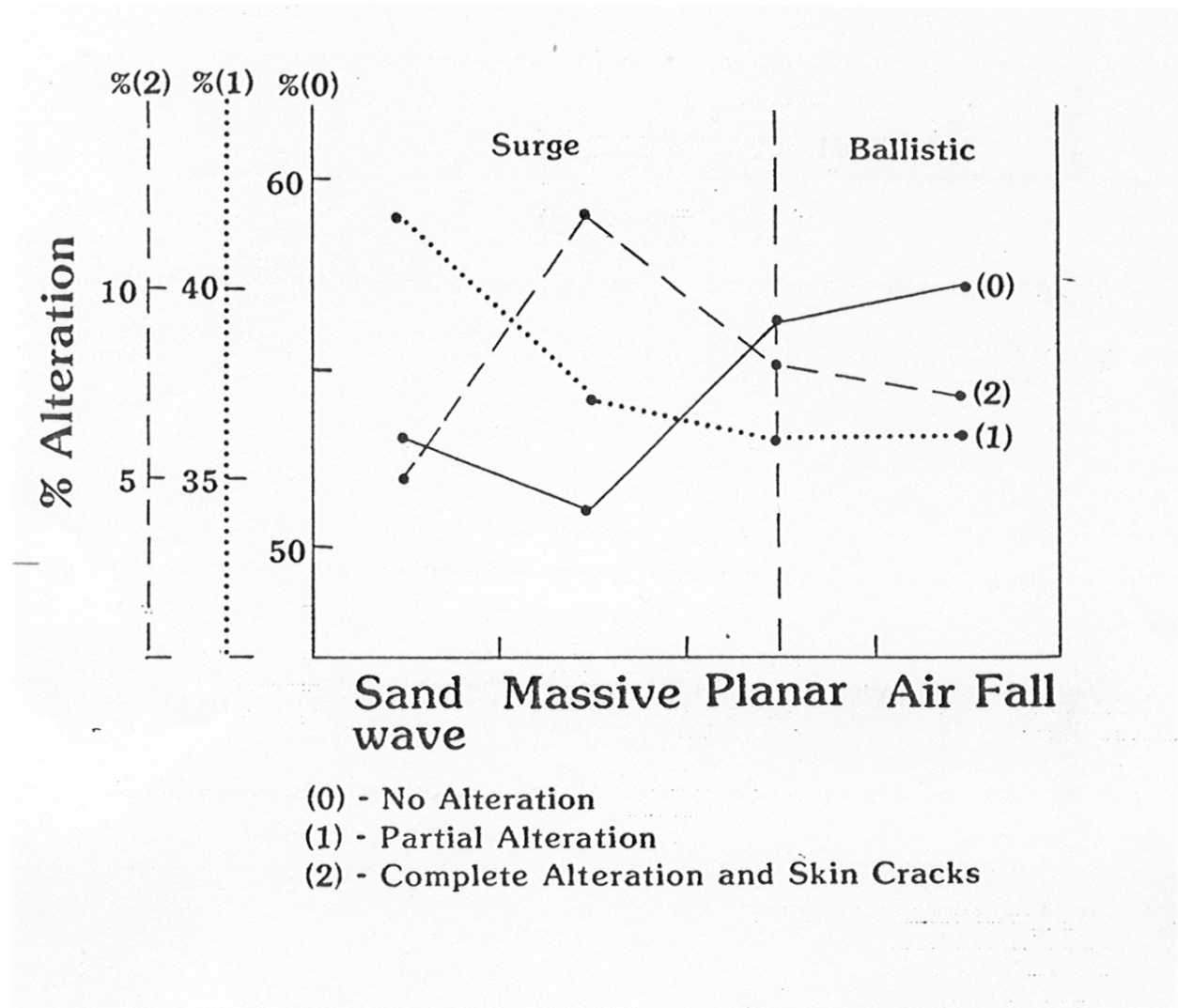


Figure 20: Plot of alteration percentage versus bed form, where (0) refers to no alteration, (1) partial alteration, and (2) complete alteration and skin cracks.

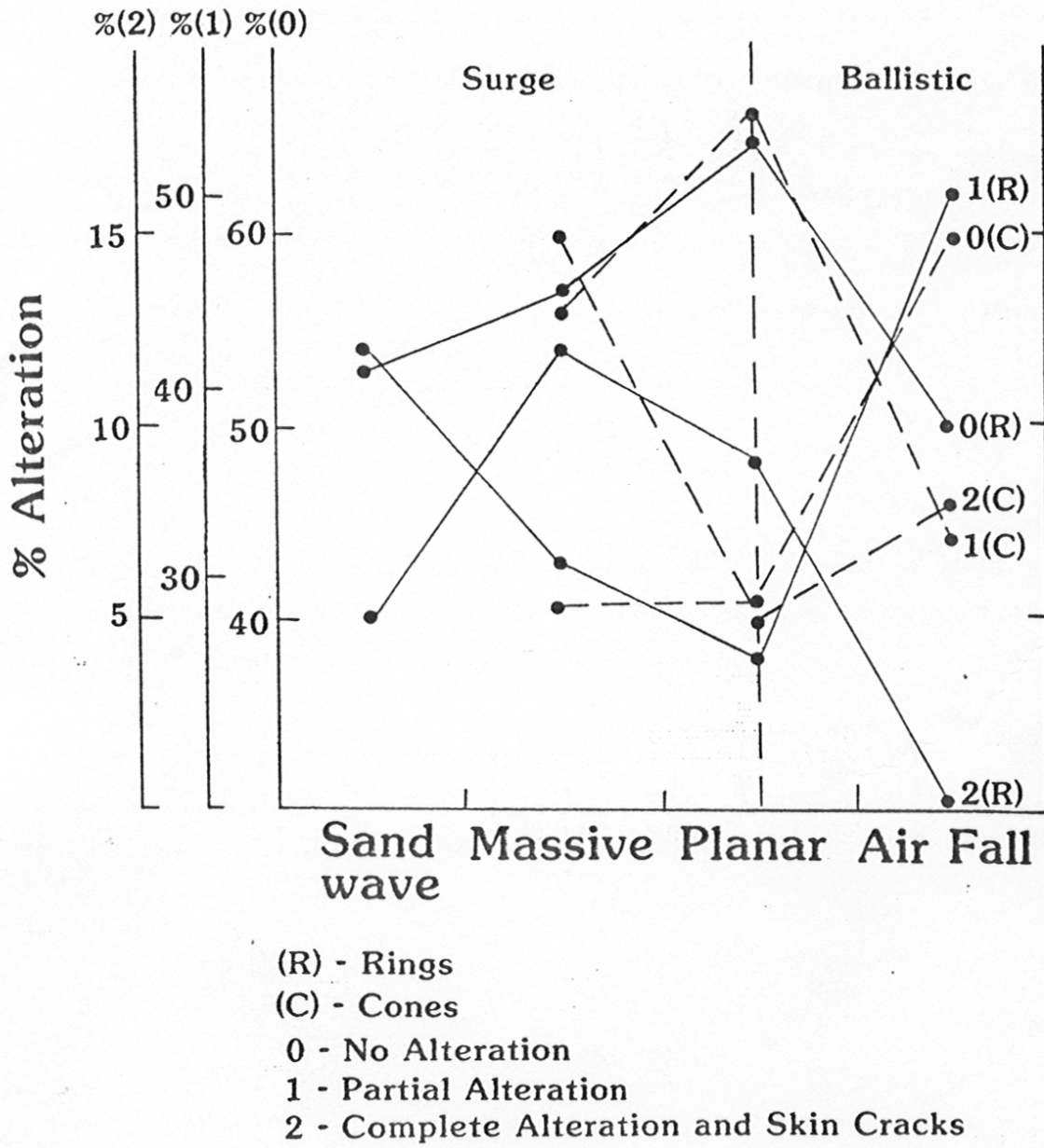


Figure 20: Plot of alteration percentage versus bed form for ash from cones (C) and rings (R)